Comparison of cadmium Cd^{2+} and lead Pb^{2+} binding by Fe_2O_3@SiO_2-EDTA nanoparticles — binding stability and kinetic studies

Amanda Kulpa[a], *Jacek Ryl*[b], *Grzegorz Skowierzak*[a], *Adrian Koterwa*[a], *Grzegorz Schroeder* [c], *Tadeusz Ossowski*[a], *Paweł Niedziałkowski*[a]*

[a] Department of Analytical Chemistry, Faculty of Chemistry, University of Gdansk, Wita Stwosza 63, 80-308 Gdansk, Gdansk (Poland)
[b] Department of Electrochemistry, Corrosion and Materials Engineering, Faculty of Chemistry, Gdansk University of Technology, Narutowicza 11/12, 80-233 Gdansk, (Poland)
[c] Faculty of Chemistry, Adam Mickiewicz University in Poznan, University of Poznan 8, 61-614 Poznan, Poland

* e-mail: pawel.niedzialkowski@ug.edu.pl (Paweł Niedziałkowski)

Received: ((will be filled in by the editorial sttaff))
Accepted: ((will be filled in by the editorial sttaff))

Abstract

This study describes the synthesis and characterization of ethylenediaminetetraacetic acid (EDTA) functionalized magnetic nanoparticles of 20 nm in size — Fe_3O_4@SiO_2-EDTA — which were used as a novel magnetic adsorbent for Cd(II) and Pb(II) binding in aqueous medium. These nanoparticles were obtained in two-stage synthesis: covering by tetraethyl orthosilicate and functionalization with EDTA derivatives. Nanoparticles were characterized using TEM, FT-IR, and XPS methods. Metal ions were detected under optimized experimental conditions using Differential Pulse Anodic Stripping Voltammetry (DPASV) and Hanging Mercury Drop Electrode (HDME) techniques.

We compared the ability of Fe_3O_4@SiO_2- EDTA to bind cadmium and lead in concentration of 553.9 $\mu g \cdot L^{-1}$ and 647.5 $\mu g \cdot L^{-1}$, respectively. Obtained results show that the adsorption rate of cadmium binding was very high. The equilibrium for Fe_3O_4@SiO_2-EDTA-Cd(II) was reached within 19 min while for the Fe_3O_4@SiO_2-EDTA-Pb(II) was reached within 25 minutes. About 2 mg of nanoparticles was enough to bind 87.5 % Cd(II) and 54.1 % Pb(II) content. In the next step the binding capacity of Fe_3O_4@SiO_2- EDTA nanoparticles was determined. Only 1.265 mg of Fe_3O_4@SiO_2- EDTA was enough to bind 96.14% cadmium ions while 5.080 mg of nanoparticles bound 40.83 % lead ions. This phenomenon proves that the studied nanoparticles bind Cd(II) much better than Pb(II). The cadmium ions binding capacity of Fe_3O_4@SiO_2-EDTA nanoparticles decreased during storage in 0.5 M KCl solution. Two days of Fe_3O_4@SiO_2-EDTA storage in KCl solution caused the 32 % increase in the amount of nanoparticles required to bind 60% of cadmium while eight-days storage caused further increase to 328 %. The performed experiment confirmed that the storage of nanoparticles in solution without any surfactants reduced their binding capacity. The best binding capacity was observed for the nanoparticles prepared directly before the electrochemical measurements.

Keywords: Fe_3O_4 nanoparticles, EDTA, surface modification of Fe_3O_4, silanization, cadmium determination

1. Introduction

Nowadays, environmental contamination by heavy metals has become one of the most important problems. Heavy metals are known as naturally occurring compounds, but the anthropogenic activities enhance their distribution in the environment. Undesirable human activity leads to their bioaccumulation in the food chains [1].

The most common heavy metal pollutants are lead, mercury, nickel, chromium, and zinc, but cadmium is regarded as the most widespread in the environment [2]. Cadmium and lead ions have negative influence on bones, liver, kidneys, lungs, brain, immunological and cardiovascular systems.

In human body, cadmium is accumulated in the kidneys and liver. Additionally, cadmium can also be found in the testes [3]. High level of cadmium concentration leads to the destruction of glomeruli and renal tubules, anaemia, bone diseases such as osteoporosis, disturbances of smell, and proteinuria [4]. Moreover, presence of cadmium ions reduces insulin secretion, affects the circulatory system, and increases lipid oxidation in the human body [5]. Cadmium induces cell death by apoptosis in the cerebral cortex [6].

In the body, lead is accumulated in soft tissues such as the liver, kidneys, lungs, brain, spleen, muscles, and heart by the blood transport. Lead is second in the list of toxic substances in the environment due to its wide distribution. Its accumulation in organism leads to saturnism [7] which causes the damage of liver and kidney [8] and reduces activities of glucose metabolism key enzymes in the brain [9].

Discovery of new, cheap, and waste-free analytical methods of determination and detection of cadmium ions in environmental samples is a great challenge. Many detection techniques have been developed for the heavy metal ion detection including: Atomic Absorption Spectroscopy (AAS) [10], Inductive Couple Plasma-Mass Spectroscopy (ICP-MS) [11], ion chromatography [12], neutron activation analysis [13], X-ray fluorescence spectroscopy (XRF) [14], and High Resolution Differential Surface Plasmon Resonance (SPR) [15].

Furthermore, electrochemical methods are often utilized for the measurement of heavy metal ions in the environment. The main advantages of these methods are simultaneous detection of multiple heavy metal ions and low detection limit capabilities [16].

The most common method used for the determination of cadmium is Differential Pulse Anodic Stripping Voltammetry (DPASV) using various electrodes such as: modified Glassy Carbon electrode (GC) [17], Hanging Mercury Drop Electrode (HMDE), a mercury film-coated electrode [18], or Boron Doped Diamond (BDD) electrode [19].

Recently, magnetic nanomaterials based on Fe_3O_4 have found many important applications in the industrial areas such as lithium-ion batteries [20,21], catalytic sorption [22] microwave absorption [23], or photocatalytic degradation [24,25]. Multifunctional magnetic nanomaterials are also extensively used in the biomedicine [23]. The most promising applications for these nanomaterials are photothermal killing of breast cancer cells [28], cell targeting and sorting [29,30], and drug delivery vehicles [31,32]. Additionally, these molecules are used in magnetic resonance [33,34] and fluorescence imaging [35,36].

Magnetic Fe_3O_4 nanoparticles can be obtained using different types of synthesis methods including: coprecipitation [37], sonochemical reaction [38], hydrothermal reaction [39], microemulsion and sol-gel synthesis [40,41], or cathodic electrochemical deposition [42]. An important characteristics of the magnetite nanoparticles is the capability of the surface modification with variety of functional groups, what enhances their applicability [43–45]. Modified surface magnetic iron oxide nanoparticles exhibit large surface area ratio toward volume and possess the ability to adsorb heavy metals in an aqueous medium throughout physical and chemical interactions [46].

Ethylenediaminetetraacetic acid (EDTA) in analytical chemistry is successfully used for the determination of many metal ions. EDTA can be also used to modify Fe_3O_4 nanoparticles to obtain superparamagnetic materials applicable for the studies on the adsorption of heavy metals [47]. Fe_3O_4@SiO_2-EDTA nanoparticles were previously obtained and they possess many advantages in comparison to EDTA. These superparamagnetic iron oxide nanoparticles have been applied as an efficient adsorbent for: methylene blue and brilliant green dyes removal from aqueous media [48], separation of rare earths [49], Cu(II), Ca(II) [50–52], Cd(II), Pb(II) [53,54], Ag(I), Mn(II), and Zn(II) [55] removal from an aqueous solution, and Hg(II) removal from an aqueous solution and crude petroleum samples [56].

In presented studies, we present a novel application approach of Fe_3O_4@SiO_2-EDTA for the cadmium detection in aqueous solution. We also compared the ability of Fe_3O_4@SiO_2-EDTA to bind cadmium and lead in minimum concentration.

The separation heavy metals with usage of magnetic nanomaterials predominant over non-magnetic materials due to the quickness and effectiveness of separation process from the medium. This work provide information about the ability of Fe_3O_4@SiO_2- EDTA to bind cadmium and lead in order

to removal them from aqueous solution by application of external magnetic field.

According to our knowledge, our study reports the electroanalytical measurements including DPV method on Hanging Drop Mercury Electrode (HDME) for the first time in the literature. Regardless of the toxicity of mercury, HDME electrode is commonly accepted in the laboratory conditions due to the repeatable and reproducible measuring results. The main reason to use this electrode was its self-renewing surface which is not available in the case of solid electrodes. Moreover, there was no risk of the electrode surface modification during each measurement.

2. Experimental

2.1. Materials

The organic solvents, potassium chloride KCl (99.9 %), cadmium nitrate tetrahydrate $Cd(NO)_3 \cdot 4H_2O$ (99.9 %), and lead nitrate $Pb(NO_3)_2$ were purchased from POCh (Poland). All chemicals applied in electrochemical measurements were used as received without further purification. Tetraethyl orthosilicate (98 %) (TEOS) and N-[(3-Trimethoxysilyl)propyl] ethylenediamine triacetic acid trisodium salt (45 %) in water were purchased from Sigma-Aldrich. Aqueous solutions were prepared using ultra-pure deionized water.

2.2. Synthesis

2.2.1. Synthesis of Fe_3O_4@SiO_2

Fe_3O_4@SiO_2 nanoparticles were obtained in three steps of synthesis. In first stage, Fe_3O_4 nanoparticles were obtained using co-precipitation method without any surfactants [57]. Then, Fe_3O_4 surface was modified by tetraethyl orthosilicate and N-[(3-trimethoxysilyl)propyl]ethylenediamine according to the procedure described below.

The 15 mL mixture of 0.02 M $FeCl_2$ and 0.04 M $FeCl_3$ ($[Fe^{2+}]$:$[Fe^{3+}]$= 1:2) was stirred in a flask under nitrogen. This was followed by the addition of 0.6 mL of 28 % ammonia solution. Upon sonication for 10 min, the reaction mixture was heated to 80 °C for 60 min. Under a neodymium magnet, the product was separated from the solution and washed until the solution reached neutral pH. In this method, Fe_3O_4 nanoparticles with a diameter of about 20 nm were obtained.

In the next process, the nanoparticles were silanized. Fe_3O_4@SiO_2 was prepared according to the Stöber method [58]. Tetraethyl orthosilicate (TEOS) was dissolved in ethanol (0.1 mL TEOS per 1 mL of ethanol). TEOS solution was slowly added to a stable suspension of Fe_3O_4 (15 mL per 1 g of Fe_3O_4), adjusted by ammonia solution to pH 11, and then the mixture was stirred overnight. The product Fe_3O_4@SiO_2 was magnetically collected, washed several times with water, and finally dried at 60 °C.

2.2.2. Synthesis of Fe_3O_4@SiO_2-EDTA nanoparticles

1 g of Fe_3O_4@SiO_2 was added to 50 mL of water and the suspension was sonicated for 30 min. 0.4 g of N-[(3-Trimethoxysilyl)propyl]ethylenediamine triacetic acid trisodium salt (45 %) in water was added to the suspension and 0.5 mL of ammonia was slowly added. The suspension was then stirred for 24 h. The product Fe_3O_4@SiO_2-EDTA was magnetically collected, washed several times with water, 0.05 M HCl, water, ethanol, and finally dried at 40 °C. Modified Fe_3O_4@SiO_2-EDTA magnetite nanoparticles were obtained. The loading of carboxyl groups present in Fe_3O_4@SiO_2-EDTA nanoparticles were determined using acid-base titration method from 0.098 mmol/g to 0.110 mmol/g [59].

2.3. Fe_3O_4@SiO_2-EDTA characterisation

Transmission electron microscopy (TEM) images of the Fe_3O_4@SiO_2-EDTA nanoparticles were obtained by Tecnai G2 Spirit BioTWIN FEI operating at 120 kV. All samples for TEM analysis were prepared by 30 min sonication of Fe_3O_4@SiO_2-EDTA nanoparticles in the absolute ethanol solution.

Fourier Transform Infrared Spectroscopy (FT-IR) spectra were obtained using Bruker FRA 106 spectrometer with the KBr pellet method.

X-ray Photoelectron Spectroscopy (XPS) was conducted using Escalab 250Xi multispectroscope (ThermoFisher Scientific, UK) utilizing monochromatic source with AlKα line at 1486.6 eV. The X-ray spot size was 250 μm. High-resolution measurements were carried out at 20 eV pass energy and 0.1 eV energy step size. Charge compensation was provided by means of a flood gun. Peak deconvolution was conducted using Avantage software provided by the spectroscope manufacturer.

2.4. Electrochemical measurements

All electrochemical measurements were carried out using mercury electrode Metrohm 663 VA Stand connected with Autolab potentiostat/galvanostat

PGSTAT-128N controlled with NOVA 2.1.4 software. The three electrode cell system consisted of Static Drop Mercury Electrode (SDME) as a working electrode, Hg/Hg_2Cl_2/ saturated KCl used as a reference electrode, and glassy carbon used as a counter electrode.

Differential pulse voltammetry (DPV) was utilized for the detection of Cd(II) and Pb(II) ions under optimized experimental conditions: deposition potential -0.9 V, deposition time 90 s, modulation amplitude 0.05 V, modulation time 0.07 s, interval time 1.85 s, and step potential 0.005 V.

The detection of Cd(II) ions was carried in a potential range of -0.8 V to -0.4 V, while for Pb(II) ions in a range of -0.65 V to -0.25 V. Metals ions solutions were prepared using cadmium and lead nitrate, pH 6.5 with potassium chloride as the supporting electrolyte. Fe_3O_4@SiO_2-EDTA nanoparticles before each measurement were prepared based on dispersion in electrolyte by sonication in ultrasonic bath for 30 min.

3. Results and Discussion

3.1. Synthesis of Fe_3O_4@SiO_2-EDTA

The magnetite derivatives called "core-shell" structures — Fe_3O_4@SiO_2-EDTA — were obtained by three-step reaction [50]. In the first step, the 20 nm magnetite nanoparticles Fe_3O_4 were obtained. In the second stage, the nanoparticles were covered with silica shell SiO_2 by reaction with tetraethyl orthosilicate (TEOS) [60]. Subsequently, their surface was modified in the reaction with N-[(3-Trimethoxysilyl)propyl]ethylenediamine tri-acetic and Fe_3O_4@SiO_2-EDTA nanoparticles were obtained (Figure 1).

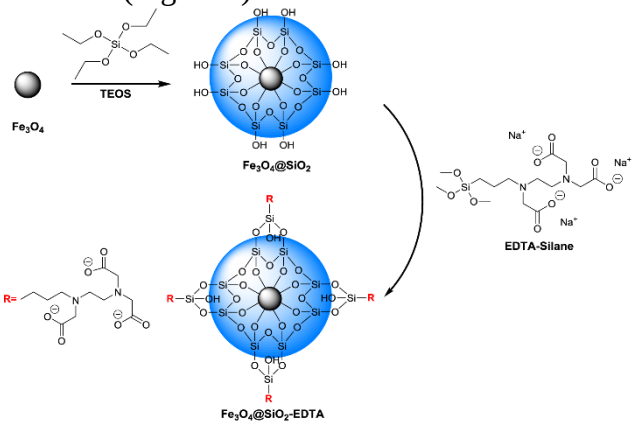

Figure 1. Scheme of Fe3O4@SiO2-EDTA synthesis.

3.2. TEM analysis

The Fe_3O_4@SiO_2-EDTA nanoparticles were characterized using Transmission Electron Microscopy. TEM images of modified magnetite nanoparticles (Figure 2) showed that the nanostructures obtained by co-precipitation method are highly homogeneous in shape and size [50]. Figure 2 a and b shows the presence of small and spherical Fe_3O_4@SiO_2- EDTA nanoparticles. The structures indicate core-shell structures. The average size of Fe_3O_4@SiO_2-EDTA nanoparticles was found to be approximately 20 nm, what is comparable to core-shell nanostructures [61]. Examined nanoparticles were found to be in the agglomerated state. This is a very common observation for magnetic nanoparticles due to their natural tendency to form agglomerates based on their magnetic nature [47].

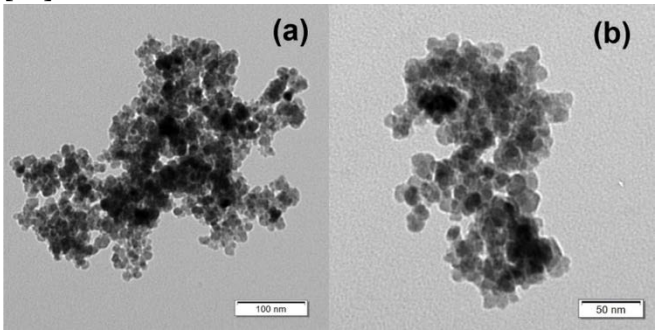

Figure 2. TEM images of a), b) Fe_3O_4@SiO_2-EDTA nanoparticles.

3.3. FT-IR analysis

The FT-IR analysis was performed for uncoated Fe_3O_4 and coated Fe_3O_4@SiO_2, and functionalized Fe_3O_4@SiO_2-EDTA nanoparticles to compare their spectroscopic differences.

All spectra were obtained in KBr pellet. The spectra obtained for Fe_3O_4 and Fe_3O_4@SiO_2 are comparable with the IR spectra described previously [62–65]. Fe_3O_4@SiO_2 EDTA nanoparticles were brown, the spectrum is of high quality, is not ragged, and the characteristic signals are present in the spectrum (Figure 3. brown line).

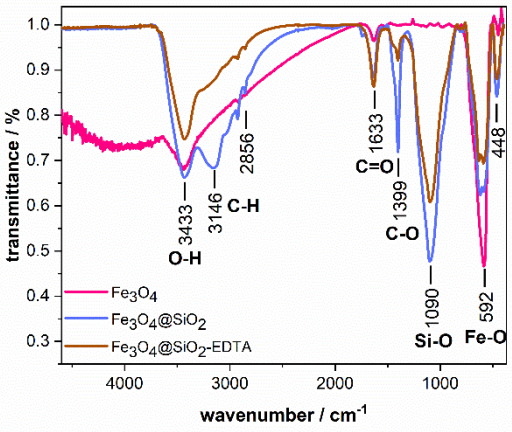

Figure 3. The FT-IR spectra of Fe_3O_4, $Fe_3O_4@SiO_2$ and studied $Fe_3O_4@SiO_2$-EDTA nanoparticles.

Figure 3. presents the comparison of unmodified Fe_3O_4 and $Fe_3O_4@SiO_2$ and modified $Fe_3O_4@SiO_2$-EDTA nanoparticles. For all analysed nanoparticles, two characteristic absorption bands appear in the wavenumber range of 420 cm^{-1} to 780 cm^{-1} for metal–oxygen bond. Stretching vibration of tetrahedral site (Fe_{tetra}-O) and octahedral site (Fe_{octa}-O) bonds are observed at 448 cm^{-1} and 592 cm^{-1}, respectively [57,62,66]. We also observed the reduction in the intensity of Fe-O band for nanoparticles coated with silica and EDTA groups. The decrease in the band intensity confirms that the nanoparticles surface was successfully modified. [50]. The presence of band at 1090 cm^{-1} confirms that the silica shell was successfully coated on Fe_3O_4 surface forming $Fe_3O_4@SiO_2$. This band relates to Si-O-C and symmetric Si-O-Si stretching vibrations [46]. The signals observed for 1399 cm^{-1} and 1633 cm^{-1} correspond to the symmetrical and asymmetrical axial deformation group -COOH, which due to vibrational motions of C–O and C=O groups [44]. The two characteristics weak bands observed in the region of 2840 cm^{-1} 2950 and strong band at 3150 cm^{-1} are found in the IR spectra for $Fe_3O_4@SiO_2$ and $Fe_3O_4@SiO_2$-EDTA (Figure 3. blue and brown lines) and correspond to the C-H bond [55]. The broad strong band at 3433 cm^{-1} corresponds to the overlapping of –OH stretching bond. This band proves the formation of hydroxyl groups on the surface of magnetite [46]. The presence of all these bonds indicate the formation of silica shell on Fe_3O_4 nanoparticles. We can concluded that the synthesis procedure was conducted successfully. Additionally, FT-IR and XPS measurements independently confirmed the presence of the EDTA groups on the nanoparticles surface.

3.4. XPS analysis

Survey XPS studies were conducted (see Figure 4a) followed by a detailed high-resolution spectral analysis in *C1s*, *O1s*, *N1s*, *Fe2p*, and *Si2p* binding energy (BE) range. The analysis to the large extent confirmed previously performed FT-IR studies. The detailed qualitative and quantitative analysis, based on high-resolution XPS spectra deconvolution, is shown in Table 1.

Peak deconvolution carried out in Fe2p binding energy range revealed presence of two oxidation states of iron, namely: Fe^{2+} (*Fe2p*$_{3/2}$ peak at 709.5 eV) and Fe^{3+} (*Fe2p*$_{3/2}$ at 711.8 eV), see Figure 4b [67,68]. The Fe^{2+}:Fe^{3+} ratio suggests the dominant presence of the lower oxidation state of iron, reaching approx. 81 %.

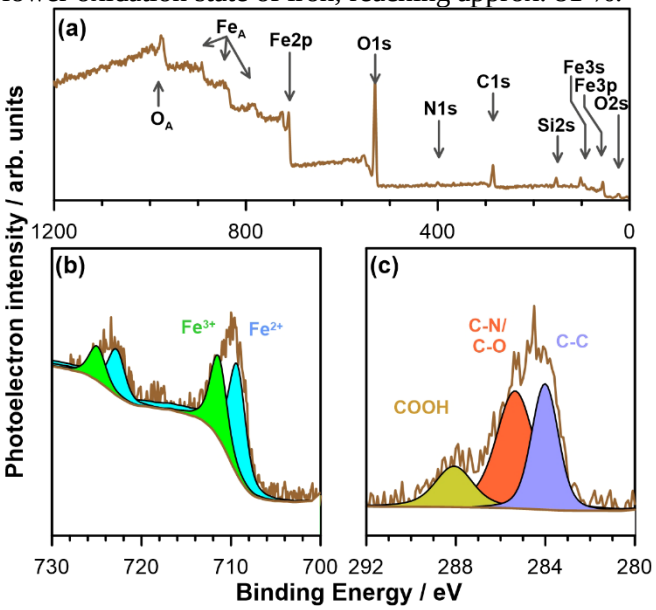

Figure 4. XPS analysis of $Fe_3O_4@SiO_2$-EDTA sample: a) survey spectra; and high-resolution spectra in b) Fe2p and c) C1s binding energy range, subjected to peak deconvolution analysis.

Furthermore, successful encapsulation of the nanoparticles with SiO_2 was confirmed by presence of the peak component in the energy range characteristic to silica at 103.5 eV [69].

The EDTA functionalization of the nanoparticles may be evaluated based on *C1s*, *O1s*, and *N1s* spectra. The nitrogen contribution is clearly visible both in survey as well as N1s spectra. A single form of nitrogen was observed peaking at 400.3 eV — a value characteristic for C-N bonds in EDTA [70].

The *C1s* spectrum was composed of three components, as presented in Figure 4c. The primary component located at 285.3 eV should be ascribed to either C-O or C-N bonds [70–72]. While the possible C-O interaction is testified by *O1s* peak at 530.7 eV,

the BE mentioned above is also characteristic for SiO_2 species which are the primary source of signal taking into consideration the stoichiometry. Hence, it should be noted that the peak located at 285.3 eV for the nanoparticles is dominated by C-N interaction (8.1 at.% is estimated based on the nitrogen content: 2.7 at.%). Next, component located at 288.2 eV should be interpreted as carbon in carboxyl species [72–74].

One should also note that the *C1s* C-N:COOH rate of 0.6:1 corroborates the estimated 0.5:1 stoichiometry based on schematic functionalization process presented on Figure 1. The third *C1s* component ascribed as C-C originates from the C-C chain in Figure 1 but also adventitious carbon contaminating the nanoparticles in atmospheric air conditions [75].

Table 1. – Chemical analysis (in at.%) of Fe_3O_4@SiO_2-EDTA sample based on the high-resolution XPS spectra deconvolution.

Chemical state	*C1s* C-C	CO/ CN	COOH	*O1s* Fe-O		C=O	*Fe2p3/2* Fe^{2+}	Fe^{3+}	*N1s* C-N	*Si2p3/2* SiO_2
BE / eV	284.4	285.3	288.2	528.8	530.7	532.3	709.5	711.8	400.3	103.5
Fe_3O_4	9.9	14.1	4.9	15.6	25.1	7.3	6.3	1.5	2.7	12.6

The three components revealed in *O1s* spectra originate from various forms of oxygen: peaks at binding energies below 530 eV are typical for metal-oxygen interaction, here Fe-O. The peak at 530.7 eV primarily originates from SiO_2 but may also come from an organic carbon. Last but not least, the highest positive shift corresponds to C=O bonds, such as in carboxylic.

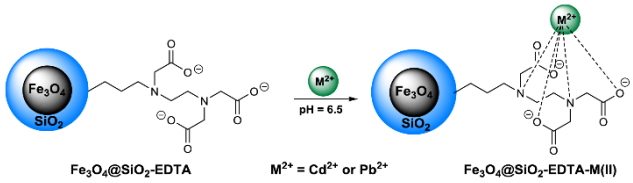

Figure 5. Scheme of proposed mechanism of Cd(II) and Pb(II) ions binding by Fe_3O_4@SiO_2- EDTA nanoparticles.

3.5. Electrochemical behaviour of Fe_3O_4@SiO_2-EDTA nanoparticles

The electrochemical properties of Fe_3O_4 nanoparticles were described previously. The modified Fe_3O_4 nanoparticles were used as modifiers of poly(vinyl)pyrrolidone (PVP) to obtain electrode meterial [76], platinum electrode for Hg(II) ions detection [56,77], carbon paste electrode detection of chlorite ions[78,79], Glassy Carbon (GC) electrode for Sudan I determination in food samples [80] or metal ions such as Cd(II), Pb(II), Cu(II) [81], and Boron Doped Diamond (BDD) electrode for the detection of a cancer biomarker [82].

The detailed binding mechanism of Fe_3O_4 modified by EDTA was described by Kataria et al. [54], while the binding mechanism of investigated ions was examined by Liu et al. and Xu et al. [50,51]. Based on this literature, all electrochemical experiments were performed in pH 6.5 due to the formation of $Cd(OH)_2$ and $Pb(OH)_2$/$Pb(OH)_4^{2-}$ hydroxides in pH higher than 7 from Cd(II) and Pb(II) ions, respectively. Furthermore, the adsorption of metal ions depends on the charge located on the nanoparticle surface [54] and the presence of EDTA groups (Figure 5). The interaction between Fe_3O_4@SiO_2-EDTA nanoparticles and metal ions involved both adsorption onto nanoparticles surface and complexation by EDTA ligand [50,53].

3.5.1. Stripping voltammetry — kinetics examination

According to our knowledge, we present here the first study of Fe_3O_4@SiO_2- EDTA using Differential Pulse Voltammetry (DPV) in combination with Hanging Drop Mercury Electrode (HDME) for binding of Cd(II) and Pb(II).

The main advantage usage of HDME is obtaining in each measurement the same repeatable results. Hanging Drop Mercury Electrode guarantee the possibility of receiving self-renewing surface of working electrode and in the same time prevents the electrode contamination by Fe_3O_4 derivatives and other ions present in solution.

Electrochemical measurements confirmed that Fe_3O_4@SiO_2-EDTA nanoparticles possess the ability to bind trace amounts of Cd(II)- and Pb(II) in an aqueous solution.

The utilisation of magnet and examined nanoparticles enable the 96.13 % removal of Cd(II) from the solution in and 54.1 % removal of Pb(II), what is confirmed with the results presented below.

Detection of Cd(II) and Pb(II) ions was carried out under optimized experimental conditions using DPASV and HDME due to reproducibility of the surface and speed of the measurement [83]. All measurements were performed in a scientific laboratory minimising the risk of the mercury environmental

contamination. DPASV involves two steps including pre-concentration and metal ions stripping. The Cd(II) and Pb(II) ions are electrodeposited onto the working electrode firstly applying a negative potential (- 0.9 V) and subsequently the faradic current obtained by oxidation is recorded when the potential sweeps toward the anodic direction (from - 0.8 V to - 0.4 V for Cd(II) and from - 0.65 V to- 0.2 V for Pb(II)).

To examine the binding abilities of Fe_3O_4@SiO_2-EDTA-Cd(II) and Fe_3O_4@SiO_2- EDTA-Pb(II) in time, a series of measurements were performed in the solution of 0.5 M KCl containing 553.9 $\mu g \cdot L^{-1}$ of Cd(II) ions and 647.5 $\mu g \cdot L^{-1}$ of Pb(II) ions, respectively. One well-defined peak at -0.62 V in anodic stripping voltammograms confirms the presence of Cd(II) ions in the solution without the nanoparticles (Figure 6 a). The peak in the potential of - 0.4 V indicates the presence of lead ions in the solution (Figure 6 b). The longest of the binding stability experiment for the nanoparticles lasted 57 minutes. The cadmium and lead ions were bound by 1.87 mg and 1.86 mg of nanoparticles, respectively. The comparison of binding abilities for Fe_3O_4@SiO_2-EDTA nanoparticles with cadmium and lead ions are presented in Figure 6 a and b, respectively. After nanoparticles addition, the cadmium peak current intensity significantly decreased after first 7 minutes. Subsequently, its intensity slightly decreased in time (Figure 6 a). The changes recorded for lead binding measurements were not so prominent. Additionally, the intensity of peak current also decreased but then slightly increased and finally reached the equilibrium. (Figure 6 b). This phenomenon confirms that the addition of Fe_3O_4@SiO_2-EDTA nanoparticles led to the increased binding of cadmium and lead ions.

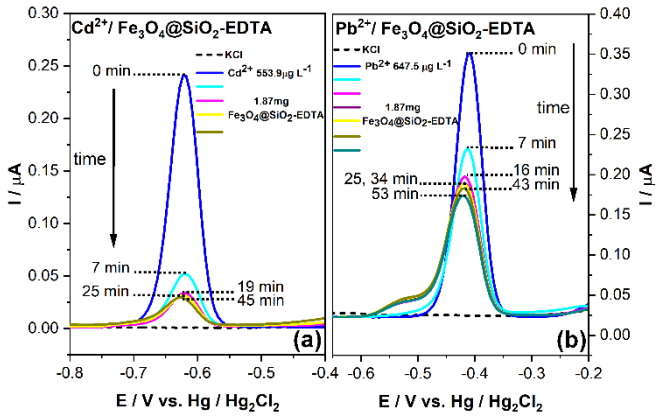

Figure 6. Anodic stripping voltammograms for the peak intensity changes over time a) for Cd(II) ions (553.9 $\mu g \cdot L^{-1}$) bound by 1.87 mg of Fe_3O_4@SiO_2-EDTA and b) for Pb(II) ions (647.5 $\mu g \cdot L^{-1}$) bound by 1.86 mg of Fe_3O_4@SiO_2-EDTA.

The degree of ions binding calculated for Fe_3O_4@SiO_2-EDTA confirms that the binding ability slightly increased and depends on time (Figure 7). The adsorption rate was high and the equilibrium was reached within 19 minutes and 25 minutes for cadmium ion and lead ion binding, respectively. The comparable amount of nanoparticles was used in these experiments. 1.87 mg of Fe_3O_4@SiO_2-EDTA was able to bind 87.5 % of Cd(II), while 1.86 mg of the nanoparticles bound 54.1 % of Pb(II). We found out that the larger amount of nanoparticles was needed to bind the lead ions. Therefore, the nanoparticles were subjected to further experiments to determine their capacity and stability in an aqueous solution.

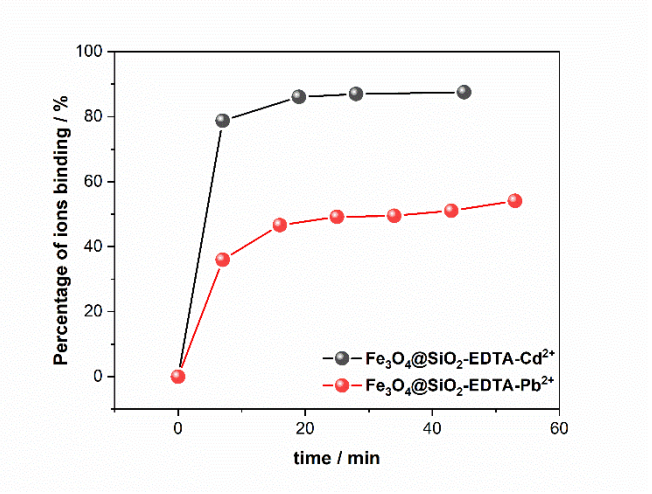

Figure 7. Comparison of binding percentage of a) Cd(II) ions (553.9 $\mu g \cdot L^{-1}$) by 1.87 mg of Fe_3O_4@SiO_2-EDTA and b) Pb(II) ions (647.5 $\mu g \cdot L^{-1}$) by 1.86 mg of Fe_3O_4@SiO_2-EDTA nanoparticles.

3.5.2. Determination of Cd (II) and Pb(II) binding capacity

To determine the metal ions binding capacity of Fe_3O_4@SiO_2-EDTA nanoparticles, we performed the anodic stripping voltammetry in 0.5 M KCl solution containing 553.9 $\mu g \cdot L^{-1}$ Cd(II) and 647.5 $\mu g \cdot L^{-1}$ Pb(II) ions. The first measurement without nanoparticles gave one peak at -0.62 V in anodic stripping voltammograms for Cd(II) (Figure 8 a) and at -0.41 V for Pb(II) (Figure 8 b).

The cadmium peak intensity decreased during titration by Fe_3O_4@SiO_2-EDTA in eight steps in amount from 0.253 mg to 2.024 mg. The obtained results show the initial linear current peak decrease for each portion of nanoparticles. After addition of 1.265 mg of nanoparticles, the equilibrium was established and another portion of nanoparticles caused no changes in current peak intensity (Fig 8 a).

A similar effect was achieved during addition of Fe_3O_4@SiO_2-EDTA nanoparticles to the Pb(II) solution. Nanoparticles were added in five steps in amount range of 1.016 mg to 5.080 mg. The Pb(II) peak intensity gently decreased after addition of each portion and after fifth step the equilibrium was not established. Due to the small changes of peak intensity and the addition of large amount of Fe_3O_4@SiO_2-EDTA nanoparticles, the measurements was stopped after the fifth step.

The gradual decrease in the peak intensity indicates the binding of the cadmium and lead ions by Fe_3O_4@SiO_2-EDTA nanoparticles. The established equilibrium proves a limited capacity of the given nanoparticles.

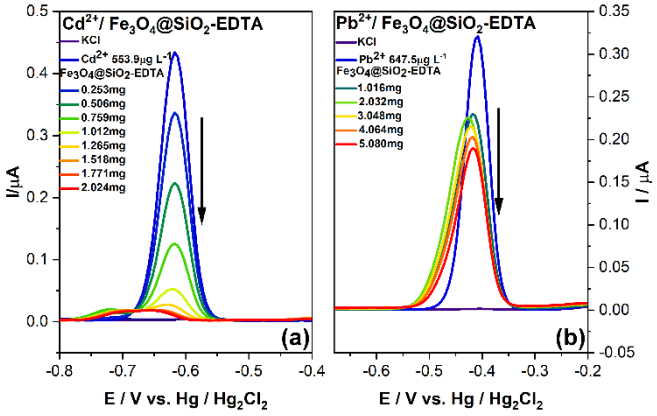

Figure 8. Anodic stripping voltammogram for binding of a) Cd(II) ions (553.9 µg·L^{-1}) and b) Pb(II) ions (647.5 µg·L^{-1}) by Fe_3O_4@SiO_2-EDTA nanoparticles.

Figure 9 shows the binding percentage for Cd(II) ions (553.9 µg·L^{-1}) and Pb(II) ions (969.0 µg·L^{-1}) by Fe_3O_4@SiO_2-EDTA nanoparticles. Cd(II) binding increases the linearity observed during addition of the subsequent Fe_3O_4@SiO_2-EDTA portions. Addition of 1.265 mg of nanoparticles caused the capturing of 96.13 % Cd(II) ions and establishing of the equilibrium. Further addition of the increased amounts of nanoparticles does not cause any changes in the bounding level.

In the case of lead ions, the Fe_3O_4@SiO_2-EDTA nanoparticles binding intensity was much lower. Addition of 5.08 mg of nanoparticles results in binding of 40.83 % of lead ions. After this step, the degree of ions binding remains at the same level. This phenomenon proves that the studied nanoparticles bind Cd(II) much better than Pb(II).

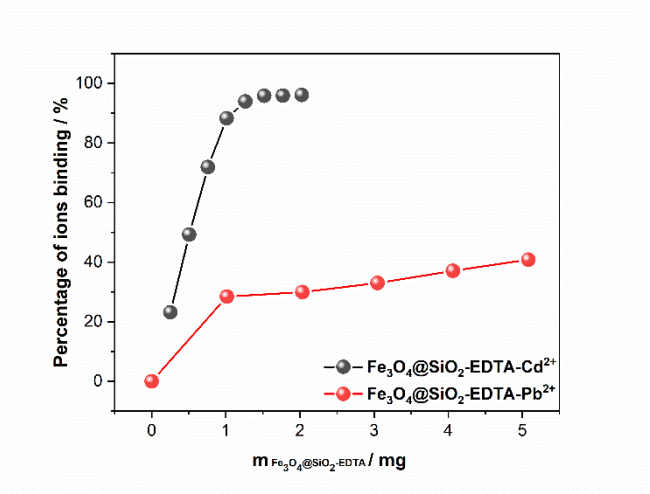

Figure 9. Percentage of Cd(II) ions (553.9 µg·L^{-1}) and Pb(II) ions 647.5 µg·L^{-1}) binding by Fe_3O_4@SiO_2-EDTA nanoparticles.

3.5.3. Determination of Fe_3O_4@SiO_2-EDTA activity

To test the activity of Fe_3O_4@SiO_2-EDTA nanoparticles, their binding capacity was determined in various time intervals: immediately after preparation, after two, and eight days. To obtain this goal, the nanoparticles were stored in a dark, cool place in the electrolyte solution (KCl 0.5 M). The experiment consisted of the anodic stripping voltammetry by addition of Fe_3O_4@SiO_2-EDTA nanoparticles portions to the cadmium solution (553.9 µg·L^{-1}) measured previously. The obtained results of Cd(II) binding activity of directly prepared solution of nanoparticles is presented at Figure 8 A. The anodic stripping voltammograms of titrated solution containing Cd(II) ions by both nanoparticles stored 2 and 8 days is shown at (Fig 10). The addition of the next portions of titrant causes a decrease in the peak intensity. A decrease of peak intensity in this case was not so profound in comparison with the freshly prepared solution.

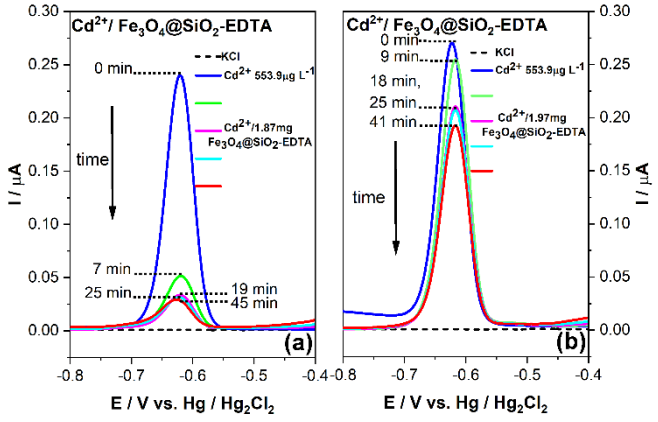

Figure 10. Anodic stripping voltammograms for binding of Cd(II) ions (553.9 μg·L^{-1}) by a) Fe_3O_4@SiO_2-EDTA after 2 days, b) Fe_3O_4@SiO_2-EDTA after 8 days of storage in the electrolyte (KCl 0.5 M) solution.

Figure 11. shows the percentage of cadmium binding for the freshly prepared solution of Fe_3O_4@SiO_2-EDTA, after 2 and 8 days of storage in the electrolyte. 2.024 mg of freshly prepared nanoparticles bound 96.13 % of Cd(II) ions from aqueous solution while after 2 days of storage 2.53 mg Fe_3O_4@SiO_2-EDTA nanoparticles is necessary to bind 95.53 % of Cd(II) ions. These results confirm that after 2 days there is a need to use 25 % more nanoparticles to bound a similar amount of Cd(II) ions, while after 8 days the binding ability of nanoparticles is much lower. To bind 60 % of Cd(II) ions present in the solution, one should use 0.623 mg of the freshly prepared Fe_3O_4@SiO_2-EDTA.

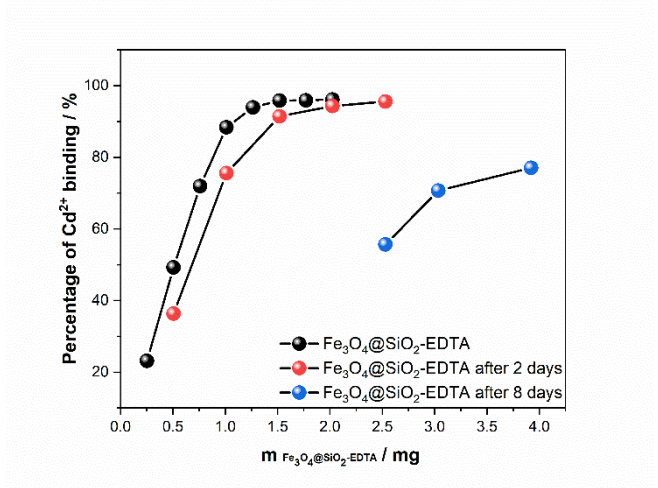

Figure 11. *Binding percentage plot of Cd(II) ions (553.9 μg·L^{-1}) by Fe_3O_4@SiO_2-EDTA for the freshly prepared solution and after 2 and 8 days of its storage in the electrolyte solution.*

After 2 days of storage the amount of nanoparticles increased to 31.6 %, with further increase to 328 % after 8 days of storage.

This experiment shows that the magnetite nanoparticles covered with EDTA groups lose their ion binding ability. This phenomenon can be associated with the strong agglomeration of Fe_3O_4@SiO_2-EDTA nanoparticles in the solution.

4. Conclusions

This study describes the preparation of Fe_3O_4 by co-precipitation method without any surfactants, by two-step modification by tetraethyl orthosilicate (TEOS), by N-[(3-Trimethoxysilyl)propyl] ethylenediamine and functionalization. Nanoparticles surface modification was confirmed by FT-IR spectra and XPS method. Additionally, the TEM characterization was performed for the obtained nanoparticles — we observed Fe_3O_4@SiO_2-EDTA nanoparticles of about 20 nm size.

Obtained nanoparticles were utilized as a Cd(II) and Pb(II) binding argent in aqueous solution. Binding ability of Fe_3O_4@SiO_2-EDTA-M(II) was conducted using DPASV method in combination with HDME in 0.5 M KCl solution. In the first stage, we compared the cadmium and lead ions binding properties of Fe_3O_4@SiO_2-EDTA. Nanoparticles showed the ability to bind both the Cd(II) and Pb(II) ions but not at the same level. For Fe_3O_4@SiO_2-EDTA-Cd(II) the adsorption rate was higher and the equilibrium was reached after 19 minutes, while in case of Fe_3O_4@SiO_2-EDTA-Pb(II) the equilibrium was not established even after 43 minutes. Binding of both cadmium and lead ions slightly depends on time. To compare these binding capacities, similar amounts of the nanoparticles were added to the Cd(II) (553.9 μg·L^{-1}) and Pb(II) (647.5 μg·L^{-1}) solutions. Electrochemical measurements results show that 87.5 % of Cd(II) ions and 54.12 % of Pb(II) ions was bound by 1.87 mg and 1.86 mg of Fe_3O_4@SiO_2-EDTA nanoparticles, respectively. We determined the binding capacity for Fe_3O_4@SiO_2-EDTA-Cd(II) and Fe_3O_4@SiO_2-EDTA-Pb(II). The experimental results indicate that only 1.265 mg and 5.080 mg of Fe_3O_4@SiO_2-EDTA is needed to bind 96.14 % of cadmium and 40.83% of lead ions, respectively. This phenomenon proves that the studied nanoparticles bind Cd(II) much better than Pb(II).

The results of the Fe_3O_4@SiO_2-EDTA nanoparticles stability tests show that the storage in 0.5 M KCl solution in dark, cool place decreases their ion binding properties. The amount of Fe_3O_4@SiO_2-EDTA to bind 60 % of Cd(II) ions after 2 and 8 days of storage increases three times in comparison with the freshly prepared nanoparticles. We observed the best

capacity for the nanoparticles prepared directly before the measurement. Furthermore, the storage of nanoparticles in potassium chloride solution significantly reduces their cadmium ions binding ability.

3. Acknowledgements

This study was financed by the University of Gdansk within the project supporting young scientists and PhD students (grant No. BMN 539-8210-B281-18). Authors would like to thank Alexander Company Gdynia for technical support.

4. References

[1] A. Butt, Qurat-ul-Ain, K. Rehman, M. X. Khan i T. Hesselberg, *Environ. Monit. Assess.*, **2018**, 190.
[2] Z. L. He, X. E. Yang i P. J. Stoffella, *J. Trace Elem. Med. Biol.*, **2005**, 19, 125–140.
[3] W. R. García-Niño i J. Pedraza-Chaverrí, *Food Chem. Toxicol.*, **2014**, 69, 182–201.
[4] K. A. James i J. R. Meliker, *Int. J. Public Health*, **2013**, 58, 737–745.
[5] M. El Muayed, M. R. Raja, X. Zhang, K. W. MacRenaris, S. Bhatt, X. Chen, M. Urbanek, T. V. O'Halloran i W. L. Lowe, Jr., *Islets*, **2012**, 4, 405–416.
[6] J. Godt, F. Scheidig, C. Grosse-Siestrup, V. Esche, P. Brandenburg, A. Reich i D. A. Groneberg, *J. Occup. Med. Toxicol. Lond. Engl.*, **2006**, 1, 22.
[7] V. Balakumar, P. Prakash, K. Muthupandi i A. Rajan, *Sens. Actuators B Chem.*, **2017**, 241, 814–820.
[8] G. Hou, M. M. Surhio, H. Ye, X. Gao, Z. Ye, J. Li i M. Ye, *Int. J. Biol. Macromol.*, **2019**, 124, 716–723.
[9] S. Yun, Y. Wu, R. Niu, C. Feng i J. Wang, *Toxicol. Lett.*, **2019**, 310, 23–30.
[10] S. Radi, S. Tighadouini, M. Bacquet, S. Degoutin, F. Cazier, M. Zaghrioui i Y. Mabkhot, *Molecules*, **2013**, 19, 247–262.
[11] R. Sánchez, J. Snell, A. Held i H. Emons, *Anal. Bioanal. Chem.*, **2015**, 407, 6569–6574.
[12] J. S. Rohrer, w *Advances in Water Purification Techniques*, Elsevier, **2019**, ss. 115–134.
[13] T. Vasilopoulou, I. E. Stamatelatos, P. Batistoni, A. Colangeli, D. Flammini, N. Fonnesu, S. Loreti, B. Obryk, M. Pillon i R. Villari, *Fusion Eng. Des.*, **2019**, 139, 109–114.
[14] L. A. Hutton, G. D. O'Neil, T. L. Read, Z. J. Ayres, M. E. Newton i J. V. Macpherson, *Anal. Chem.*, **2014**, 86, 4566–4572.
[15] S. Wang, E. S. Forzani i N. Tao, *Anal. Chem.*, **2007**, 79, 4427–4432.
[16] C. Ariño, N. Serrano, J. M. Díaz-Cruz i M. Esteban, *Anal. Chim. Acta*, **2017**, 990, 11–53.
[17] M. Baghayeri, H. Alinezhad, M. Fayazi, M. Tarahomi, R. Ghanei-Motlagh i B. Maleki, *Electrochimica Acta*, **2019**, 312, 80–88.
[18] E. Fischer, *Anal. Chim. Acta*, **1999**, 8.
[19] K. E. Toghill, L. Xiao, G. G. Wildgoose i R. G. Compton, *Electroanalysis*, **2009**, 21, 1113–1118.
[20] S. Zhou, Y. Zhou, W. Jiang, H. Guo, Z. Wang i X. Li, *Appl. Surf. Sci.*, **2018**, 439, 927–933.
[21] L. Guo, H. Sun, C. Qin, W. Li, F. Wang, W. Song, J. Du, F. Zhong i Y. Ding, *Appl. Surf. Sci.*, **2018**, 459, 263–270.
[22] J. R. Rajabathar, J. J. Vijaya, A. Prabakaran, Z. A. Issa, A. M. Atta, A. O. Ezzat, A. M. Al-Mayouf i H. A. Al-Lohedan, *J. Alloys Compd.*, **2017**, 698, 1077–1085.
[23] M. Qiao, X. Lei, Y. Ma, L. Tian, W. Wang, K. Su i Q. Zhang, *J. Alloys Compd.*, **2017**, 693, 432–439.
[24] Q. Sun, Y. Hong, Q. Liu i L. Dong, *Appl. Surf. Sci.*, **2018**, 430, 399–406.
[25] Q. Zhang, L. Yu, C. Xu, J. Zhao, H. Pan, M. Chen, Q. Xu i G. Diao, *Appl. Surf. Sci.*, **2019**, 483, 241–251.
[26] A. Pariti, P. Desai, S. K. Y. Maddirala, N. Ercal, K. V. Katti, X. Liang i M. Nath, *Mater. Res. Express*, **2014**, 1, 35023.
[27] R. Hao, R. Xing, Z. Xu, Y. Hou, S. Gao i S. Sun, *Adv. Mater.*, **2010**, 22, 2729–2742.
[28] G. A. Sotiriou, F. Starsich, A. Dasargyri, M. C. Wurnig, F. Krumeich, A. Boss, J.-C. Leroux i S. E. Pratsinis, *Adv. Funct. Mater.*, **2014**, 24, 2818–2827.
[29] Z.-H. Sun, L.-H. Zhou, G.-J. Deng, M.-B. Zhegn, W.-Q. Yan, W.-J. Li, L.-T. Cai i P. Gong, *Chin. J. Anal. Chem.*, **2017**, 45, 1427–1433.
[30] R. Di Corato, N. C. Bigall, A. Ragusa, D. Dorfs, A. Genovese, R. Marotta, L. Manna, T. Pellegrino, *ACS Nano*, **2011**, 5, 1109–1121.
[31] C. Wang, L. Huang, S. Song, B. Saif, Y. Zhou, C. Dong i S. Shuang, *Appl. Surf. Sci.*, **2015**, 357, 2077–2086.
[32] G. Bao, S. Mitragotri i S. Tong, *Annu. Rev. Biomed. Eng.*, **2013**, 15, 253–282.
[33] J.-H. Liu, L. Wang, T.-Q. Zhang, J.-Q. Wang, X. Gong, F.-Z. Cui, J.-J. Zheng, B. Li i Z. Shi, *Chin. J. Anal. Chem.*, **2019**, 47, 678–685.

[34] J. Qin, H. Peng, J. Ping i Z. Geng, *Mater. Res. Bull.*, **2019**, 114, 90–94.
[35] N. Mir, P. Karimi, C. E. Castano, N. Norouzi, J. V. Rojas i R. Mohammadi, *Appl. Surf. Sci.*, **2019**.
[36] C.-L. Huang, W.-J. Hsieh, C.-W. Lin, H.-W. Yang i C.-K. Wang, *Ceram. Int.*, **2018**, 44, 12442–12450.
[37] H. Meng, Z. Zhang, F. Zhao, T. Qiu , J. Yang, *Appl. Surf. Sci.*, **2013**, 280, 679–685.
[38] D. Ghanbari, M. Salavati-Niasari i M. Ghasemi-Kooch, *J. Ind. Eng. Chem.*, **2014**, 20, 3970–3974.
[39] V. Madhubala i T. Kalaivani, *Appl. Surf. Sci.*, **2018**, 449, 584–590.
[40] O. M. Lemine, K. Omri, B. Zhang, L. El Mir, M. Sajieddine, A. Alyamani i M. Bououdina, *Superlattices Microstruct.*, **2012**, 52, 793–799.
[41] D. Zhang, Z. Tong, S. Li, X. Zhang, A. Ying, *Mater. Lett.*, **2008**, 62, 4053–4055.
[42] M. Aghazadeh, I. Karimzadeh i M. R. Ganjali, *J. Magn. Magn. Mater.*, **2017**, 439, 312–319.
[43] F. Ke, J. Jiang, Y. Li, J. Liang, X. Wan, S. Ko, *Appl. Surf. Sci.*, **2017**, 413, 266–274.
[44] W. Cai, M. Guo, X. Weng, W. Zhang, Z. Chen, *Mater. Sci. Eng. C*, **2019**, 98, 65–73.
[45] X. Liu, J. Tian, Y. Li, N. Sun, S. Mi, Y. Xie, Z. Chen, *J. Hazard. Mater.*, **2019**, 373, 397–407.
[46] D. Chen, T. Awut, B. Liu, Y. Ma, T. Wang, I. Nurulla, *E-Polym.*, **2016**, 0.
[47] A. G. Magdalena, I. M. B. Silva, R. F. C. Marques, A. R. F. Pipi, P. N. Lisboa-Filho i M. Jafelicci, *J. Phys. Chem. Solids*, **2018**, 113, 5–10.
[48] N. Kataria i V. K. Garg, *Environ. Res.*, **2019**, 172, 43–54.
[49] D. Dupont, J. Luyten, M. Bloemen, T. Verbiest i K. Binnemans, *Ind. Eng. Chem. Res.*, **2014**, 53, 15222–15229.
[50] Y. Liu, R. Fu, Y. Sun, X. Zhou, S. A. Baig i X. Xu, *Appl. Surf. Sci.*, **2016**, 369, 267–276.
[51] M. Xu, Y. Zhang, Z. Zhang, Y. Shen, M. Zhao i G. Pan, *Chem. Eng. J.*, **2011**, 168, 737–745.
[52] Y. Liu, M. Chen i H. Yongmei, *Chem. Eng. J.*, **2013**, 218, 46–54.
[53] Y. Huang i A. A. Keller, *Water Res.*, **2015**, 80, 159–168.
[54] N. Kataria i V. K. Garg, *Chemosphere*, **2018**, 208, 818–828.
[55] E. Ghasemi, A. Heydari i M. Sillanpää, *Microchem. J.*, **2017**, 131, 51–56.
[56] U. Condomitti, A. Zuin, A. T. Silveira, K. Araki i H. E. Toma, *J. Electroanal. Chem.*, **2011**, 661, 72–76.
[57] C. Atila Dinçer, N. Yıldız, N. Aydoğan i A. Çalımlı, *Appl. Surf. Sci.*, **2014**, 318, 297–304.
[58] W. Stöber, A. Fink i E. Bohn, *J. Colloid Interface Sci.*, **1968**, 26, 62–69.
[59] F. Nemati, M. M. Heravi i R. Saeedi rad, *Chin. J. Catal.*, **2012**, 33, 1825–1831.
[60] D. Lewandowski, M. Cegłowski, M. Smoluch, E. Reszke, J. Silberring i G. Schroeder, *Microporous Mesoporous Mater.*, **2017**, 240, 80–90.
[61] Z. Chen, Z. Geng, Z. Zhang, L. Ren, T. Tao, R. Yang i Z. Guo, *Eur. J. Inorg. Chem.*, **2014**, 2014, 3172–3177.
[62] T. Q. Bui, H. T. M. Ngo i H. T. Tran, *J. Sci. Adv. Mater. Devices*, **2018**, 3, 323–330.
[63] M. Chellappa i U. Vijayalakshmi, *Mater. Today Proc.*, **2019**, 9, 371–379.
[64] L. Wang, C. Shen i Y. Cao, *J. Phys. Chem. Solids*, **2019**, 133, 28–34.
[65] M. Nasrollahzadeh, M. Sajjadi i H. A. Khonakdar, *J. Mol. Struct.*, **2018**, 1161, 453–463.
[66] B. Unal, M. S. Toprak, Z. Durmus, H. Sözeri i A. Baykal, *J. Nanoparticle Res.*, **2010**, 12, 3039–3048.
[67] A. Mohammed, M. Saracoglu, N. El-Bagoury, T. Sharshar, M. Ibrahim, J. Wysocka, S. Krakowiak i J. Ryl, *Int. J. Electrochem. Sci.*, **2016**, 11, 1–23.
[68] D. Wilson i M. A. Langell, *Appl. Surf. Sci.*, **2014**, 303, 6–13.
[69] N. Koshizaki, H. Umehara i T. Oyama, *Thin Solid Films*, **1998**, 325, 130–136.
[70] S. Ravi, S. Zhang, Y.-R. Lee, K.-K. Kang, J.-M. Kim, J.-W. Ahn i W.-S. Ahn, *J. Ind. Eng. Chem.*, **2018**, 67, 210–218.
[71] M. C. Ortega-Liebana, N. X. Chung, R. Limpens, L. Gomez, J. L. Hueso, J. Santamaria i T. Gregorkiewicz, *Carbon*, **2017**, 117, 437–446.
[72] J. Wysocka, M. Cieślik, S. Krakowiak i J. Ryl, *ELECTROCHIMICA ACTA*, **2018**.
[73] E. Johansson i L. Nyborg, *Surf. Interface Anal.*, **2003**, 35, 375–381.
[74] J. Ryl, R. Bogdanowicz, P. Slepski, M. Sobaszek i K. Darowicki, *J. Electrochem. Soc.*, **2014**, 161, H359–H364.
[75] S. Evans, *Surf. Interface Anal.*, **1997**, 25, 924–930.
[76] P. Tipsawat, U. Wongpratat, S. Phumying, N. Chanlek, K. Chokprasombat i S. Maensiri, *Appl. Surf. Sci.*, **2018**, 446, 287–292.
[77] L. Yang, X. Ren, F. Tang i L. Zhang, *Biosens. Bioelectron.*, **2009**, 25, 889–895.
[78] E. Al-Zahrani, M. T. Soomro, R. M. Bashami, A. U. Rehman, E. Danish, I. M. I. Ismail, M. Aslam i A. Hameed, *J. Environ. Chem. Eng.*, **2016**, 4, 4330–4341.

[79] H. Beitollahi, S. Tajik i S. Jahani, *Electroanalysis*, **2016**, 28, 1093–1099.
[80] H. Yin, Y. Zhou, X. Meng, T. Tang, S. Ai i L. Zhu, *Food Chem.*, **2011**, 127, 1348–1353.
[81] F. Bai, X. Zhang, X. Hou, H. Liu, J. Chen i T. Yang, *Electroanalysis*, **2019**, 31, 1448–1457.
[82] M. Braiek, Y. Yang, C. Farre, C. Chaix, F. Bessueille, A. Baraket, A. Errachid, A. Zhang i N. Jaffrezic-Renault, *Electroanalysis*, **2016**, 28, 1810–1816.
[83] A. Profumo, D. Merli i M. Pesavento, *Anal. Chim. Acta*, **2005**, 539, 245–250.